Valence instability and crystal structures in $YbCu_xGa_{2-x}$ studied by x-ray absorption spectroscopy and x-ray diffraction

Hitoshi Yamaoka [1,*] Yuichi Michiue [2] Yoshiya Yamamoto [3,†] Naohito Tsujii [4,‡] Masashi Arita [5] Hitoshi Sato [5] Masahiro Sawada [5] Hirofumi Ishii [6] Nozomu Hiraoka [6] and Jun′ichiro Mizuki [3,§]

[1] *RIKEN SPring-8 Center, 1-1-1 Kouto, Sayo, Hyogo 679-5148, Japan*
[2] *International Center for Materials Nanoarchitectonics (MANA), National Institute for Materials Science, 1-2-1 Sengen, Tsukuba, Ibaraki 305-0047, Japan*
[3] *Graduate School of Science and Technology, Kwansei Gakuin University, Sanda, Hyogo 669-1337, Japan*
[4] *International Center for Materials Nanoarchitectonics, National Institute for Materials Science, Sengen 1-2-1, Tsukuba, 305-0047, Japan*
[5] *Hiroshima Synchrotron Radiation Center, Hiroshima University, Higashi-Hiroshima, Hiroshima 739-0046, Japan*
[6] *National Synchrotron Radiation Research Center, Hsinchu 30076, Taiwan*

(Dated: April 15, 2024)

The electronic and crystal structures of $YbCu_xGa_{2-x}$ under pressure were investigated by high-resolution x-ray absorption spectroscopy (XAS) at the Yb-L_3 absorption edge and x-ray diffraction. First-order valence transition was found in $YbCu_{0.5}Ga_{1.5}$ around 5 GPa accompanying the structural phase transition. In YbCuGa and $YbCu_{1.5}Ga_{0.5}$ the Yb valence increased gradually up to 5–7 GPa and 16 GPa with pressure, respectively, and did not show a significant change above those pressures. XAS study at the Cu-L absorption edge was also performed. The major hybridization partner of Yb $4f$ electrons switched from Ga to Cu with increasing the Cu content around $x = 1$–1.5, where the c–f hybridization was weakest. Photoelectron spectroscopy was performed around Yb $4d$–$4f$ resonance energy and at 8.4 eV.

I. INTRODUCTION

Material properties strongly correlate to the degree of freedom of electrons such as spin, orbital, and charge. In intermetallic compounds, valence fluctuation provides an additional degree of freedom induced by pressure or temperature. The rare-earth intermetallic compounds of Ce, Sm, Eu, and Yb systems have often shown valence fluctuation, which depends on the hybridization between the localized $4f$ electrons and itinerant conduction electrons (c–f hybridization) and the hybridization strength is characterized by the Kondo Temperature (T_K) [1]. The physical property of the compounds is described within a frame of Doniach phase diagram where the interplay between the Ruderman-Kittel-Kasuya-Yosida (RKKY) interaction and the Kondo effect has been observed [2–6]. In the vicinity at which both interactions compete is called a quantum critical point (QCP) where a magnetic phase transition is suppressed and anomalous and exotic physical properties such as unconventional superconductivity or non-Fermi liquid state have been observed.

Ce- and Yb-containing ternary intermetallics of RE-M-X (RE = Ce, Yb, M = transition metal, X = main group) often reveal the intermediated valence state. In Yb-containing ternary intermetallics, Yb-M gallides have been extensively studied for the past three decades, for example in YbTGa (T = Mg, Cu, Pd, Ag, Pt, Au) [7–12], $YbAgGa_2$ [11, 13], $YbAu_xGa_{2-x}$ [14], $YbCu_{5-x}Ga_x$ [15], $YbCuGa_3$ [16], $YbNiGa_4$ [11, 17], $YbNi_3Ga_9$ [18–22], $Yb_2Ru_3Ga_{10}$ [23] and $Yb_2Pt_6Ga_{15}$ [24]. Among them, the Yb-Cu-Ga and Yb-Ni-Ga systems have attracted much interest because of their interesting physical properties such as heavy fermion behavior, mixed valence, and quantum criticality induced by chemical substitution or pressure. While most works have been focused on the synthesis of new samples and the study of the transport properties such as resistivity, specific heat, and magnetic susceptibility with x-ray diffraction (XRD) patterns to determine the crystal structures.

Pressure could control T_K and induce evolution from nonmagnetic fermi liquid to magnetic state through QCP. High-pressure studies have been performed for YbAuGa [11], $YbAgGa_2$ [11, 13], $YbNi_3Ga_9$ [18–20], $YbNiGa_4$ [11, 17]. Electronic structures are also important to clarify the origin of the physical properties. However, studies of the electronic structures were limited to $Yb_2Pt_6Ga_{15}$ [24] at ambient pressure and $YbAgGa_2$ [13], $YbNiGa_4$ [11, 17], $YbNi_3Ga_9$ [20, 21], and $YbNi_3Ga_9$ [20] under pressure. Pressure dependence of the detailed electronic structure has not been explored even for the most simple YbTGa systems.

YbCuGa is known to also show valence fluctuation with an orthorhombic $CeCu_2$-type crystal structure [7, 8]. Magnetic susceptibility showed a broad maximum of around 190 K [8], which corresponded to the Kondo energy of 205 K measured by the inelastic neutron scattering [9]. Thermoelectric power also showed a minimum of around the same temperature range [8]. The

* Corresponding author: hitoshi_yamaoka@mineo.jp; Present address: Institute for R&D Promotion, Doshisha University, Kyoto 602-8580, Japan
† Present address: Nagoya Institute of Technology, Nagoya, Aichi, 466-8555 Japan
‡ Corresponding author: TSUJII.Naohito@nims.go.jp
§ Present address: Center for Research Initiative, Kwansei Gakuin University, Sanda, Hyogo 669-1337, Japan

mean Yb valence was estimated to be 2.61 from the fit to the magnetic susceptibility with the interconfiguration fluctuation (ICF) model [8]. Electrical resistivity (ρ) of the Fermi liquid follows a relation $\rho = \rho_0 + AT^2$, where ρ_0, A, and T are residual resistivity attributed to impurity scattering, coefficient attributed to electron–electron scattering, and temperature, respectively. In YbCuGa T^2-dependence of the electrical resistivity was observed at 4.2–92 K and thus Fermi liquid ground state was suggested [8]. A-coefficient of the T^2-dependence was estimated to be 0.0025 $\mu\Omega$cm/K^2 [9].

In the Yb system, the Kondo temperature decreases with pressure, and the Yb valence shifts to Yb^{3+}, and Yb^{3+} should become dominant in the pressure range above QCP. But in YbCuGa no measurement of the electronic structure was reported even at ambient pressure so far. In YbCuGa, it is also not known which of Cu or Ga would be a main partner of the hybridization with Yb.

In this study, we prepared samples with different composition ratios of Cu and Ga, $YbCu_xGa_{2-x}$, and clarified the composition dependence of the electronic structure and the hybridization as well, systematically. We also studied the pressure dependence of their electronic structures and discussed the possibility of quantum criticality. We employed a high-resolution x-ray absorption spectroscopy with partial fluorescence mode (PFY-XAS) at the Yb-L_3 absorption edge [25–27]. We found the first-order transition of the Yb valence in $YbCu_{0.5}Ga_{1.5}$ around 5 GPa and the successive transitions in YbCuGa and $YbCu_{1.5}Ga_{0.5}$. Crystal structures of $YbCu_xGa_{2-x}$ under pressure have not been explored. We performed XRD study under pressure to ascertain whether the valence transition was accompanied by a structural phase transition. The first-order valence transition in Yb of $YbCu_{0.5}Ga_{1.5}$ accompanied the structural phase transition. Photoelectron spectroscopy (PES) and XAS at the Cu-L absorption edge were performed at ambient pressure.

II. EXPERIMENTS

Polycrystalline samples of $YbCu_xGa_{2-x}$ ($x = 0.5$, 0.8, 1.0, and 1.5) were prepared by melting in sealed niobium tubes and subsequent annealing. Stoichiometric amounts of pure elements of Yb (99.9%), Cu (99.99%), and Ga (99.99%) were sealed in Nb tubes by arc under an Ar atmosphere. The Nb tubes were sealed in evacuated quartz tubes, and were heated in an electric furnace at 1373 K for 3 hours and were further annealed at 973 K for 96 hours. These compounds have the orthorhombic KHg_2-type crystal structure with the space group of $Imma$. The Cu and Ga atoms are distributed on the 8c sites. Chemical compositions measured with electron probe micro-analyzer were $Yb_{1.05}Cu_{0.5}Ga_{1.5}$ for $x = 0.5$, $Yb_{1.05}Cu_{0.8}Ga_{1.2}$ for $x = 0.8$, $Yb_{1.05}CuGa$ for $x = 1.0$, and $Yb_{0.92}Cu_{1.5}Ga_{0.5}$ for $x = 1.5$. Afterwards, we denote the Yb composition as 1.0 for simplicity.

Pressure dependence of the x-ray diffraction patterns was measured at Taiwan beamline BL12B2, SPring-8, using a three-pin plate diamond anvil cell (DAC, Almax Industries) with a CCD detection system at room temperature. We take an arrangement of both incoming and outgoing x-ray beams passing through the diamonds with an incident photon energy of $h\nu = 18$ keV ($\lambda = 0.6888$ Å). A two-dimensional image of the CCD system was integrated by using the FIT2D program [28]. The diffraction patterns were analyzed by the JANA2006 program [29, 30].

PFY-XAS measurements were performed at room temperature at the Taiwan beamline BL12XU, SPring-8. Details of the experimental setup have been published elsewhere [31, 32]. The overall energy resolution was estimated to be about 1 eV around the emitted photon energy of 7400 eV from the elastic scattering. The high-pressure conditions were realized using a diamond anvil cell (DAC) with a Be-gasket and the pressure-transmitting medium was silicone oil. A membrane-controlled DAC was used for high-pressure experiments. The pressure was measured based on the Raman shift of the ruby fluorescence [33–35].

Soft x-ray PES was performed at the beamline BL-7, the Hiroshima Synchrotron Radiation Center (HiSOR), equipped with a hemispherical electron-energy analyzer (Gammadata-Scienta SES-2002). In the soft x-ray PES the energy resolution (ΔE) was set to 40–50 meV around $h\nu = 182$ eV under the vacuum pressure below 10^{-8} Pa. The Fermi edge of Au on the sample holder was used to calibrate the binding energy. Samples were fractured in vacuum just before the measurements. The energy resolution and the Fermi level are determined with a fit of the Fermi edge of Au using a convolution of Gaussian and

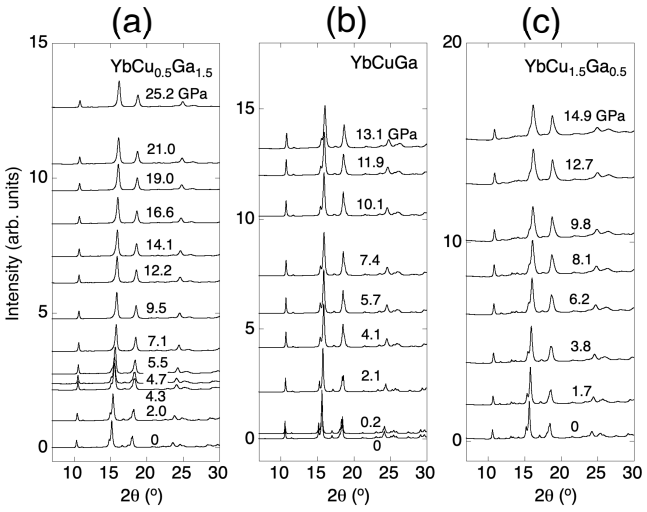

FIG. 1. (Color online). X-ray diffraction patterns of (a) $YbCu_{0.5}Ga_{1.5}$, (b) YbCuGa, and (c) $YbCu_{1.5}Ga_{0.5}$ at 300 K. The baseline height of each pattern scales to the measured pressure.

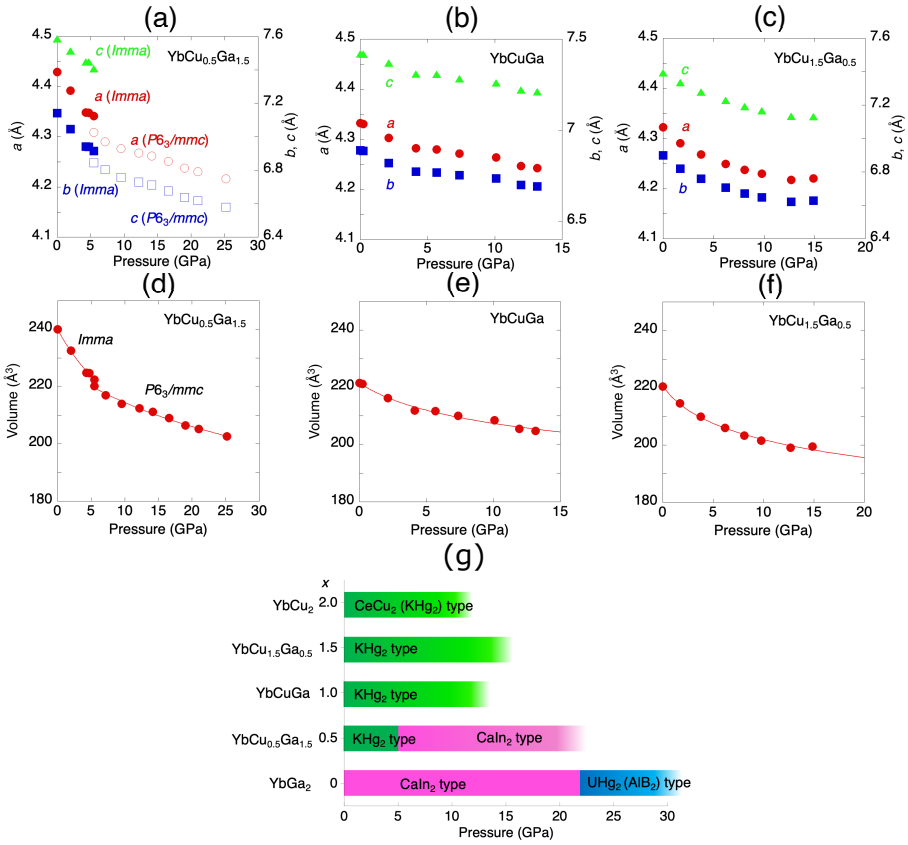

FIG. 2. (Color online) (a)–(c) Pressure dependence of the lattice constants of (a) $YbCu_{0.5}Ga_{1.5}$, (b) YbCuGa, and (c) $YbCu_{1.5}Ga_{0.5}$. (d)–(f) Pressure dependence of the volume of (d) $YbCu_{0.5}Ga_{1.5}$, (e) YbCuGa, and (f) $YbCu_{1.5}Ga_{0.5}$. Solid lines are the fits by using the empirical formula of the Murnaghan's equation of state [41]. (g) A summary of the pressure dependence of the type of the crystal structure in $YbCu_xGa_{2-x}$. $YbGa_2$ has a structural phase transition at 22 GPa [39]. The maximum pressures measured here were approximately 25, 13, and 15 GPa for $YbCu_{0.5}Ga_{1.5}$, YbCuGa, and $YbCu_{1.5}Ga_{0.5}$, respectively.

Fermi-Dirac functions. XAS study at the Cu-L absorption edge was performed at BL-14, HiSOR with the total electron yield mode, where the samples were fractured under the vacuum [36]. The energy resolution around 930 eV was set to be approximately 0.15 eV. It is noted that we could discuss the relative shift of the energy an order of magnitude lower than the resolution.

III. RESULTS

A. X-ray diffraction

Figure 1 shows XRD patterns as a function of pressure for $YbCu_{0.5}Ga_{1.5}$, YbCuGa, and $YbCu_{1.5}Ga_{0.5}$. $YbCu_{0.5}Ga_{1.5}$ shows a phase transition at the pressure between 5.5 and 7.1 GPa.

$RCu_{0.8}Ga_{1.2}$ and $RCu_{0.5}Ga_{1.5}$ (R = Tm, Lu, both sides in the periodic table) were reported to have the crystal structures of KHg_2 type (space group $Imma$) and $CaIn_2$ type (space group $P6_3/mmc$), respectively [37]. For the case of R = Yb, $YbCu_{0.8}Ga_{1.2}$ has been reported to be of the KHg_2 type, similar to the case of R = Tm and Lu. For $YbCu_{0.5}Ga_{1.5}$, there is no report, but the XRD pattern shows that the KHg_2 type is the most plausible. This is probably due to the large ionic radius of Yb due to valence fluctuation or the effect of the number of valence electrons in $YbCu_{0.5}Ga_{1.5}$. It may be reasonable that the crystal structure of $YbCu_{0.5}Ga_{1.5}$ undergoes a phase transition to the $CaIn_2$ type when approaching the Yb^{3+} state with pressure.

Diffraction data of YbCuGa and $YbCu_{1.5}Ga_{0.5}$ at all pressures were fitted by the structure model isotypic to $YbCu_{0.8}Ga_{1.2}$, which is the KHg_2-type structure of the space group $Imma$ [37]. As for $YbCu_{0.5}Ga_{1.5}$, the KHg_2-type structure was taken at 4.74 GPa and below, while the diffraction patterns at 7.13 GPa and above were fitted by the model isotypic to $LuCu_{0.5}Ga_{1.5}$; namely, the $CaIn_2$-type structure of the space group $P6_3/mmc$ [37]. The pattern at 5.46 GPa resembles that at 7.13 GPa, but was insufficiently fitted by the $CaIn_2$-type model. Residual intensities were seen in the lower-angle region of the

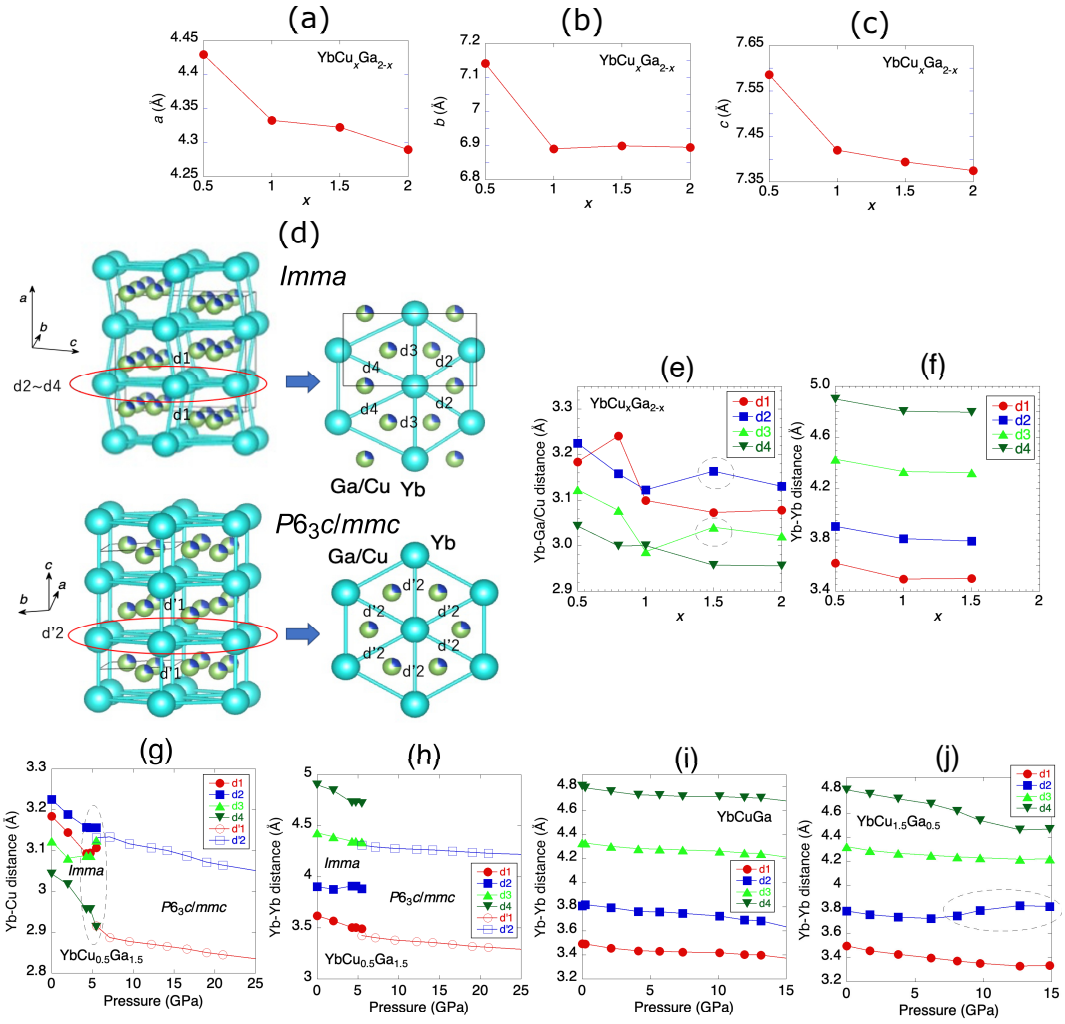

FIG. 3. (Color online) (a)–(c) Chemical composition (x) dependence of the lattice constants at ambient pressure. The errors are within the size of the symbols. (d) Crystal structures and definition of the distances from $d1$ to $d4$ for the crystal structure of $Imma$ type and $d'1$ and $d'2$ for that of $P6_3/mmc$ type, where d is the distance between Yb and M (Ga, Yb). (e)–(f) x dependence of the atomic distances of (e) Yb-Ga/Cu and (f) Yb-Yb estimated from the present XRD results. Note that the distances at $x = 0.8$ and 2.0 were estimated from the CIFs (Crystallographic Information Files) of $YbCu_2$ and $YbCu_{0.8}Ga_{1.2}$ in the Inorganic Crystal Structure Database [37]. In (e) Dotted circles correspond to the data where pressure-induced anomalous changes occurred. (g)–(h) Pressure dependence of the atomic distances of (g) Yb-Cu and (h) Yb-Yb in $YbCu_{0.5}Ga_{1.5}$. (i)–(j) Pressure dependences of the atomic distances of Yb-Yb are shown for (i) YbCuGa and (j) $YbCu_{1.5}Ga_{0.5}$. In (j) dotted circle corresponds to the data where anomalous change was observed. In (e)–(j) the errors are within the size of the symbols.

strong reflection peak at around 15.5°, which indicated the coexistence of the KHg_2-type structure. Thus, the diffraction pattern at 5.46 GPa was well fitted by assuming that the sample consists of two phases of $CaIn_2$ and KHg_2 types. Examples of the plots of the profile fitting are given in the Supplemental Material (Figure S1) [38]. The results of structure refinements and final parameters are also summarized in Tables. S1–S4 in the Supplemental Material [38].

Figures 2 (a)–2 (f) show the pressure dependence of the lattice constants and the volume. YbCuGa and $YbCu_{1.5}Ga_{0.5}$ kept the KHg_2-type structure up to approximately 13 and 15 GPa, respectively. While $YbCu_{0.5}Ga_{1.5}$ has a structural phase transition approximately at 5 GPa. Pressure-induced decrease of the lattice constants and the volume of $YbCu_{0.5}Ga_{1.5}$ is more rapid at the pressure less than 5 GPa compared to those of others and they become gradual after the structural transition as shown in Fig. 2 (d). In Fig. 2 (g) we summarize the pressure dependence of the type of the crystal structure in $YbCu_xGa_{2-x}$ including $YbGa_2$ [39]. $YbGa_2$ has a $CaIn_2$-type crystal structure at ambient pressure, while $YbCu_xGa_{2-x}$ has the KHg-type crystal structure with the space group of $Imma$ at $x \geq 0.5$ ($x = 0.5$, 1.0, 1.5, and 2.0). Pressure dependence of the crystal structure for $YbCu_2$ was recently measured [40].

In Figs. 2 (d)-2 (f) we show fits of the pressure-volume relation by using the empirical formula of the Murnaghan's equation of state widely used in the high-pressure research [41], $\frac{V}{V_0} = [1 + p\frac{B_0{}'}{B_0}]^{-\frac{1}{B_0{}'}}$, where V, V_0, B_0, and $B_0{}'$ are volume, volume at ambient pressure, bulk modulus, and its first derivative with respect to the pressure, respectively. We obtain the parameters of B_0 = 43.9 GPa, $B_0{}'$ = 18.7, V_0 = 220.7 Å^3 for $YbCu_{1.5}Ga_{0.5}$ and B_0 = 66.4 GPa, $B_0{}'$ = 22.1, V_0 = 221.6 Å^3 for YbCuGa. In $YbCu_{0.5}Ga_{1.5}$ the parameters are estimated to be B_0 = 54.8 GPa, $B_0{}'$ = 6.84, V_0 = 240.0 Å^3 at $p < 6$ GPa and B_0 = 121 GPa, $B_0{}'$ = 8.85, V_0 = 228.1 Å^3 at $p > 5$ GPa.

B. Lattice constants and atomic distances

In Fig. 3 (a)–3 (c) we show x dependence of the lattice constants. x dependence of them is small at $x \geq 1.0$. Figure 3 (d) shows the crystal structures of the KHg_2-type with the space group $Imma$ and the $CaIn_2$-type with the space group $P6_3/mmc$. We estimated the atomic distances between Yb and M (Ga, Cu) at ambient pressure based on the results in Fig. 2, as shown in Fig. 3 (e). Crystallographically, there is only one site occupied by Cu and Ga in the model of space group $Imma$. We assumed that this site is M, Cu and Ga randomly occupy (solid solution) the M site (at a ratio corresponding to the composition ratio of the sample). There are 12 relatively short-range M sites around one Yb. It means that M has 12 coordinates to Yb as shown in Fig. 3 (d). These 12 interatomic distances (Yb–M) are classified into 4 types from $d1$ to $d4$, and there are 2 each for $d1$ and $d3$, and 4 for $d2$ and $d4$, 12 distances in total. They are the averaged distances of Yb–Cu and Yb–Ga. Therefore, in this case, the Yb–Cu and Yb–Ga distances in the crystal cannot be determined separately from the XRD analysis. Figure 3 (e) is a plot of the above four types of Yb–M distances against the parameter x. The CIFs (Crystallographic Information Files) of $YbCu_2$ and $YbCu_{0.8}Ga_{1.2}$ were found in ICSD (the Inorganic Crystal Structure Database) [42] and the interatomic distances calculated from them were also added. There is a trend that the distances decrease with increasing x. However, in $d1$ at $x = 0.8$ and $d2$ and $d3$ at $x = 1.5$, the Yb-M distance increases irregularly. Furthermore, the decrease of the atomic distances in $d1$ and $d4$ seems to slow down between $x = 1.5$ and 2. Here, the data at $x = 0.8$ estimated based on the table [37] seem not to be closely connected to the present measured results and thus, we do not discuss the anomaly of the Yb–M distances at $x = 0.8$. In Fig. 3 (f) we show the atomic distances between Yb atoms against x. The Yb-Yb distance decreases monotonically with x.

Figure 3 (g) shows the pressure dependence of the Yb–M distances in $YbCu_{0.5}Ga_{1.5}$. In the high-pressure phase of the $P6_3/mmc$ type, $YbCu_{0.5}Ga_{1.5}$ has one independent Yb site crystallographically. There are 12 M (= Cu or Ga) sites in the vicinity of Yb, and the distance between Yb and M is divided into two types ($d'1$ and $d'2$) each containing 6 atoms. In the $P6_3/mmc$ crystal structure, the change in the interatomic distance is relatively gradual and well corresponds to the contraction of the unit cell in Fig. 2 (d) and gradual change in the Yb valence after the valence transition in Fig. 4 (f) below. We observed the anomaly of the Yb–Cu distances just below the pressure range of the phase transition. Figure 3 (h) shows the pressure dependence of the Yb–Yb distances in $YbCu_{0.5}Ga_{1.5}$. The Yb–Yb distances show smooth changes before and after the phase transition, compared to the case of the Yb–Cu distance.

Figures 3 (i) and 3 (j) show the pressure dependences of the distances between the Yb atoms in YbCuGa and $YbCu_{1.5}Ga_{0.5}$, respectively. The distances between Yb atoms decrease monotonically with pressure. But there is an exception in Fig. 3 (j) that the $d2$ in $YbCu_{1.5}Ga_{0.5}$ increases above 10 GPa as shown in Fig. 3 (j) although both the crystal structure and the Yb valence do not show any anomaly around 10 GPa.

C. Pressure dependence of Yb valence

Pressure dependence of the PFY-XAS spectra was measured at room temperature as a function of pressure for $YbCu_{0.5}Ga_{1.5}$, YbCuGa, and $YbCu_{1.5}Ga_{0.5}$ as shown in Figs. 4 (a)–4 (d). Figure 4 (e) shows an example of the fits to the PFY-XAS spectrum of $YbCu_{0.5}Ga_{1.5}$ at 5.0 GPa. In the fits, we assumed some Voigt functions for each Yb component with the arctan-like backgrounds. The mean valence is defined to be v=2 + I(3+)/(I(2+) + I(3+)), where I(n+) is the intensity of Yb^{n+} component [43]. The errors of the valence are on the order of ±0.01. In $YbCu_{0.5}Ga_{1.5}$ we found the first-order valence transition as shown in Fig. 4 (f). In YbCuGa and $YbCu_{1.5}Ga_{0.5}$the Yb valence increased gradually up to 5–7 GPa and 16 GPa with pressure, respectively, and did not show a significant change above those pressures as shown in Figs. 4 (g) and 4 (h).

In Figs. 4 (g) and 4 (h) we approximate the pressure dependence of the Yb valence by a modified logistic curve which draws an S-shaped curve and the increase approaches nearly a constant value at high pressures [38]. The logistic curve has been used widely to represent many natural phenomena. Here, we define the pressure of the inflection point of the fit curves as the critical pressure of the valence crossover (P_v) for the pressure-induced successive valence transition. We also use P_v for the first-order valence transition.

In $YbCu_{0.5}Ga_{1.5}$ we observed a rapid increase of the Yb valence up to 5 GPa with pressure and after the valence transition, the Yb valence does not change much. We also measured the PFY-XAS spectra by decreasing the pressure as shown in Fig. 4 (b). The results show a hysteresis of the pressure-induced change in the Yb valence in Fig. 4 (f), indicating the first-order valence tran-

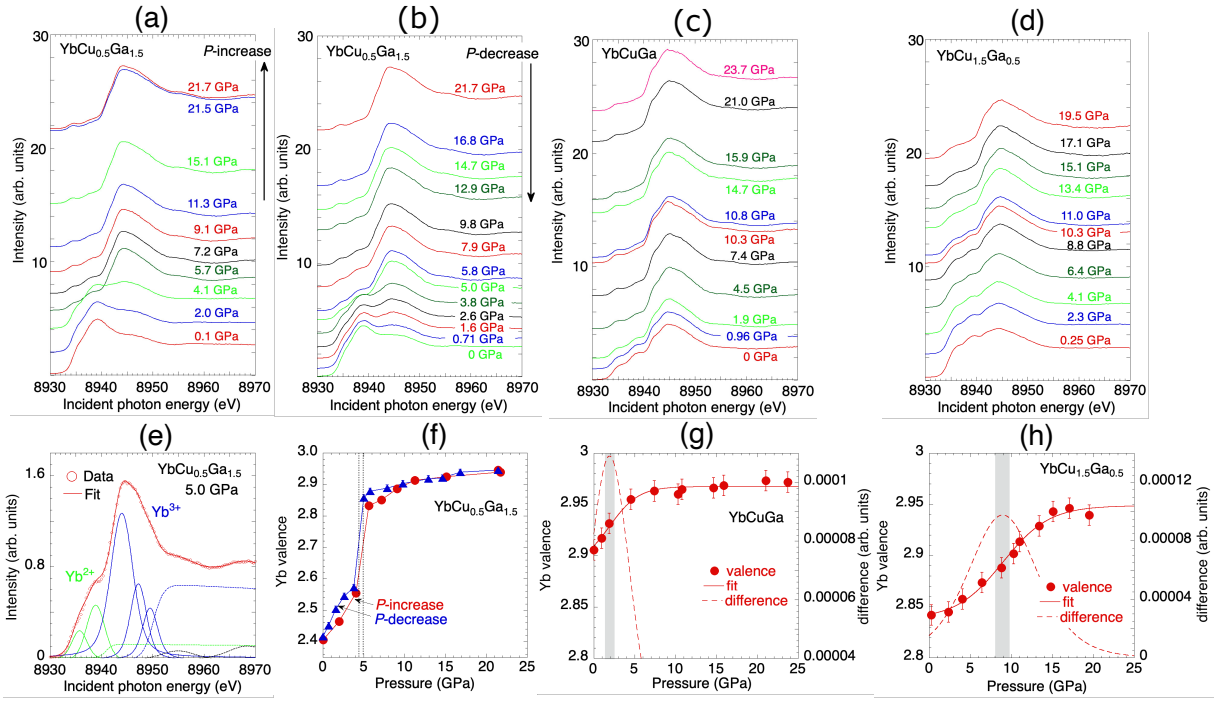

FIG. 4. (Color online) (a)–(d) Pressure dependence of the PFY-XAS spectra of (a) $YbCu_{0.5}Ga_{1.5}$ with increasing the pressure, (b) $YbCu_{0.5}Ga_{1.5}$ with decreasing the pressure, (c) YbCuGa, and (d) $YbCu_{1.5}Ga_{0.5}$ at room temperature. The baseline height of each spectrum scales to the measured pressure. (e) An example of the fit to the PFY-XAS spectrum at 5.0 GPa of $YbCu_{0.5}Ga_{1.5}$. (f)–(h) Pressure dependence of the Yb valence of (f) $YbCu_{0.5}Ga_{1.5}$, (g) YbCuGa, and (h) $YbCu_{1.5}Ga_{0.5}$. The errors of the valence are on the order of ± 0.01. In (f) closed circles and closed triangles correspond to the Yb valences when the pressure is increased and decreased, respectively. In (g) and (h) solid lines, dashed lines, and shaded areas are fit to the Yb valence using the modified logistic curve, differential of the fitted curves, and critical pressure rages of the valence transition, respectively.

sition. The valence transition pressure coincides with the structural phase transition observed in the XRD spectra. Therefore, this valence transition originates from the structural phase transition. Meanwhile, in the other two compounds of YbCuGa and $YbCu_{1.5}Ga_{0.5}$ no structural phase transition was observed as described above. Mean Yb valences at the ambient pressure were estimated to be 2.46 for $YbCu_{0.5}Ga_{1.5}$, 2.91 for YbCuGa, and 2.84 for $YbCu_{1.5}Ga_{0.5}$, where the errors are on the order of ± 0.01. This value for YbCuGa is in contrast to the value of 2.61 estimated from the fit to the magnetic susceptibility with the ICF model by Adroja *et al.* [8] The ICF model assumed the thermal population of two different valence states. However, the inelastic neutron scattering showed the Kondo energy of 205 K [9], suggesting the dominant role of the Kondo interaction on the Yb valence state through the hybridization between f and conduction electrons. Therefore, the value of the Yb valence based on the ICF model may be underestimated.

In $YbCu_xGa_{2-x}$ the lattice constants and the unit cell volume increase with decreasing the Cu content x at ambient pressure. On the other hand, the critical transition pressure seems not to correlate to the change in the lattice constants and the volume. Furthermore, the Yb valence increases with increasing x up to $x = 1.0$, does not show a remarkable change between $x = 1.0$ and 1.5, but decreases rapidly between $x = 1.5$ and 2.0 at ambient pressure. We discuss the chemical composition dependence of the Yb valence in detail in the Discussion below.

D. XAS spectra at the Cu-L absorption edge and the valence band spectra

We measured the XAS spectra at the Yb-L_3 absorption edge with those at the Cu-L absorption edge at low temperatures. Photoelectron spectroscopy was also performed at low temperatures.

Figure 5 (a) shows the comparison of the PFY-XAS spectra for $YbCu_{0.5}Ga_{1.5}$, YbCuGa, and $YbCu_{1.5}Ga_{0.5}$ at 10 K at the Yb-L_3 absorption edge. The intensity is normalized by the area. In $YbCu_{0.5}Ga_{1.5}$ divalent Yb component is dominant, while in $YbCu_{1.5}Ga_{0.5}$ and YbCuGa the intensity of the trivalent Yb component becomes stronger.

We also measured the XAS spectra of Cu at the Cu-L absorption edge and at 12 K with the total flu-

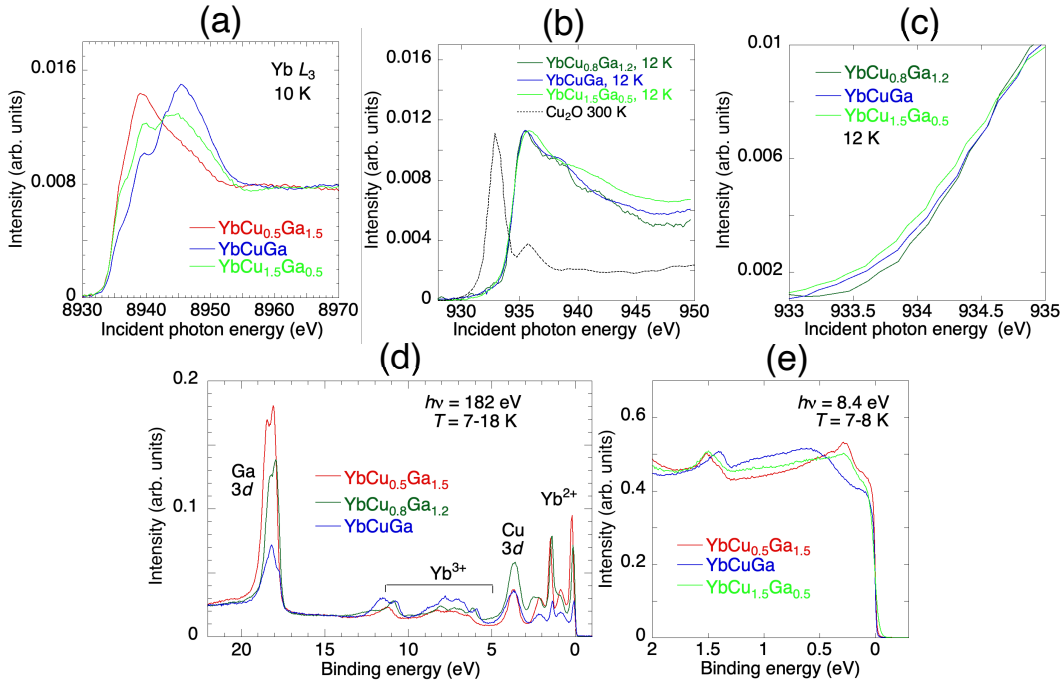

FIG. 5. (Color online) (a) PFY-XAS spectra of $YbCu_{1.5}Ga_{0.5}$, YbCuGa, and $YbCu_{0.5}Ga_{1.5}$ at 10 K and at the Yb-L_3 absorption edge. (b) X-ray absorption spectra of $YbCu_{0.8}Ga_{1.2}$, YbCuGa, and $YbCu_{1.5}Ga_{0.5}$ at the Cu K absorption edge and 12 K with that of Cu_2O at 300 K for comparison. (c) Enlarged figure of (b) near the absorption edge. (d) Valence band spectra of $YbCu_{0.5}Ga_{1.5}$, $YbCu_{0.8}Ga_{1.2}$, and YbCuGa at $h\nu = 182$ eV and 7–18 K. (e) Valence band spectra of $YbCu_{0.5}Ga_{1.5}$, YbCuGa, and $YbCu_{1.5}Ga_{0.5}$ near the Fermi level at the incident photon energy $h\nu = 8.4$ eV (Xe lamp) and 7–8 K.

orescence yield mode for $YbCu_{1.5}Ga_{0.5}$, YbCuGa, and $YbCu_{0.8}Ga_{1.2}$ as shown in Fig. 5 (b). The intensity is normalized to the peak. In Fig. 5 (b) we also show the spectra of Cu_2O ($3d^{10}$) at 300 K as a reference. The spectrum of Cu_2O reproduced well the previous results [44]. The absorption edges of $YbCu_xGa_{2-x}$ shift to higher energies than those of CuO ($3d^9$) and Cu_2O [44–46], where Cu atoms are covalently bonded to the O atoms, but similar to that of the metallic compound of $YbInCu_4$ [47]. Theoretical calculations for fcc and bcc Cu metal suggested that the first peak at 935 eV and the second peak at 939 eV corresponding to the transitions of $2p$–$3d$ and $2p$–$3s$, respectively [45]. Figure 5 (b) indicates that the XAS spectra at the Cu-L absorption edge do not show a significant difference among the above three samples. Figure 5 (c) shows an expanded view of Fig. 5 (b) around the absorption edge. Relative energy shift of the absorption edge to lower incident energy was observed as increasing the Cu content x.

Figure 5 (d) shows valence band spectra measured at $4d$–$4f$ resonant energy of 182 eV and at 7–18 K [48, 49]. The spectra consist of Yb^{2+} near the Fermi level and Yb^{3+} components with Cu $3d$ and Ga $3d$ peaks. The intensity of the Yb^{3+} component in YbCuGa is stronger than those in others, while the intensities of the Yb^{2+} component in $YbCu_{0.5}Ga_{1.5}$ and $YbCu_{0.8}Ga_{1.2}$ are stronger than that in YbCuGa When the intensity of the Yb^{2+} component is strong, the c–f hybridization is also usually strong in the Kondo system. Therefore, above results indicate stronger hybridization in $YbCu_{0.5}Ga_{1.5}$ and $YbCu_{0.8}Ga_{1.2}$ than that in $YbCu_{0.5}Ga_{1.5}$. This trend agrees with the results of the PFY-XAS as shown in the x dependence of the Yb valence in Fig. 6 (b) below.

Bulk-sensitive high-resolution PES was also performed by using light of 8.4 eV from a Xe lamp at 7–8 K for $YbCu_{0.5}Ga_{1.5}$, YbCuGa, and $YbCu_{1.5}Ga_{0.5}$ as shown in Fig. 5 (e). The peaks near the Fermi level and 1.5 eV are the components of $4f_{7/2}$ and $4f_{5/2}$, respectively. It is noted that in this incident photon energy range, the cross-section of the Yb $4f$ electrons is much smaller compared to that of Cu/Ga d and p electrons and, therefore, the valence band spectra mainly reflect the d and p states [50]. The density of states (DOS) at the Fermi level of YbCuGa is smaller than those of $YbCu_{0.5}Ga_{1.5}$ and $YbCu_{1.5}Ga_{0.5}$. The Yb valence of YbCuGa is closer to the Yb^{3+} state compared to the other samples, suggesting a weaker hybridization strength in YbCuGa than that in $YbCu_{0.5}Ga_{1.5}$ and $YbCu_{1.5}Ga_{0.5}$. In Yb metal and Yb compounds, pressure induces the shift of the Yb^{2+} component toward the Fermi level, charge transfer occurs above the Fermi level, the intensity of Yb^{2+} component decreases, and a transition to the Yb^{3+} state occurs normally [51, 52]. In YbCuGa the Yb valence is already near the Yb^{3+} state at ambient pressure and, therefore,

it is reasonable that the transition pressure to the Yb^{3+} state for YbCuGa lower than those for $YbCu_{0.5}Ga_{1.5}$ and $YbCu_{1.5}Ga_{0.5}$ as shown in Fig. 4. Additionally, we measured the valence band spectra of $YbCu_{0.5}Ga_{1.5}$ around the Yb $4d$–$4f$ resonant energy. Details are shown in Fig. S3 of the supplemental Material [38].

IV. DISCUSSION

A. Chemical composition dependence

The chemical composition dependence of the volume is shown in Fig. 6 (a). The volume decreases rapidly between $x = 0.5$ and 1.0 and does so gradually between $x = 1.0$–2.0. The chemical composition dependence of the Yb valence estimated from the PFY-XAS and the valence band spectra at ambient pressure between $x = 0.5$–1.5 is shown in Fig. 6 (b), with the data at $x = 0$ measured at 0.6 GPa [39], at $x = 2.0$ estimated from the valence band spectrum [53], and at $x = 2.0$ previously measured from the XAS spectrum [40]. The Yb valences derived from the valence band spectra show a trend to be larger than those from the PFY-XAS spectra. The Yb valence derived from the valence band spectra may remain the surface effect although we separate the surface component of the Yb^{2+} spectra [54]. The decrease of the Cu content induced the increase of the c–f hybridization at $x \leq 1$, resulting in the decrease of the Yb valence. As shown in Fig. 5 (c), the spectra at the Cu-L absorption edge showed a shift to the lower incident energy with increasing the Cu content x between $x = 0.8$–1.5. A similar energy shift of the Cu absorption edge was observed in $YbInCu_4$ in the temperature-induced valence transition, where it has been considered that the charge transfer occurred between Yb and Cu [47, 55]. The result of the energy shift of the Cu-L absorption edge supports the charge transfer with the increase of the Yb valence up to $x = 1.0$–1.5 in Fig. 6 (b).

The atomic distances between Yb and M (M = Ga, Cu), the lattice constants, and the volume decreased with increasing x, the Cu content [38]. Here, the Yb valence increased with increasing the Cu content x at $x \leq 1$, suggesting the decrease of the c–f hybridization between Yb and Ga. It is reasonable to consider that the electron transfer may occur mainly between Yb $4f$ and Ga bands at $x \leq 1$ and the decrease of the Ga DOS may cause the decrease of the hybridization of Yb and Ga [38]. The Yb valence increases with decreasing the volume normally. Thus, both effects of the decreases of both the Ga DOS and the volume result in the increase of the Yb valence up to $x = 1.0$. Interestingly, in the region where Cu and Ga contents are comparable, the hybridization is the weakest and the Yb valence approaches 3+. On the other hand, the Yb-M distances of $d2$ and $d3$ show an anomalous increase at $x = 1.5$ as shown in Fig. 3 (e) (indicated by dotted circles). The atomic distances of $d1$ and $d4$ show a little change between $x = 1.5$–2.0 and also the volume decreases with x gradually at $x \geq 1.0$. These changes in the atomic distances at $x \geq 1.5$ seem to correlate to those in the Yb valences in Fig. 6 (a).

Additionally, we note that in $YbAu_xGa_{2-x}$ a similar trend as in $YbCu_xGa_{2-x}$ was reported where the Yb valence took the maximum around $x \sim 1$ which correlated to the minimum of the volume [14]. However, in $YbCu_xGa_{2-x}$ the minimum of the volume does not correspond to the maximum of the Yb valence.

The atomic distances of $d1$ and $d4$ changed irregularly at $x \geq 1.5$ as described above with increasing the Cu content, but we should, on the other hand, consider the fact that both the lattice constants and volume decreased as a whole with increasing x. Therefore, the sudden large decrease of the Yb valence at $x = 2.0$ is anomalous. Another factor could be also considered as the origin of the rapid decrease of the Yb valence and increase of the hybridization at $x = 2.0$. At $x \geq 1.5$ the c–f hybridization between Yb $4f$ and Cu d may be enhanced largely because of both the effects of the increase of the Cu d DOS and the decrease of the Yb–Cu atomic distances. Our preliminary DFT calculation results (not considering hybridization) support this scenario that increasing x makes Cu d DOS much stronger in particular at $x \geq 1.5$ [38]. Further detailed calculations taking into account the hybridization remain challenging in the future. Thus, in $YbCu_xGa_{2-x}$ the hybridization partner of Yb switched from Ga to Cu with increasing the Cu content around $x = 1.0$–1.5, where the hybridization became minimum.

B. Pressure dependence

Figure 6 (c) shows the chemical composition and pressure dependences of the Yb valence in $YbCu_xGa_{2-x}$. The Yb valence of $YbGa_2$ is included as a reference although it has a different crystal structure of $CaIn_2$ at ambient pressure [39]. In $YbGa_2$ Schwartz *et al.* [39] measured the pressure dependence of the XAS spectra at the Yb-L_3 absorption edge at three pressure points of 0.6, 4.7, and 28.8 GPa, but the values of the Yb valence were not estimated. Here, we analyzed their data and added the estimated values of the Yb valences in Figs. 6 (b) and 6 (c) [38].

It is known that in most Yb compounds the magnetic order occurs at relatively high Yb valence values of more than 2.7 [56]. YbCuGa showed already a relatively high Yb valence of 2.91 at ambient pressure. However, YbCuGa was considered to be in the Fermi liquid ground state at ambient pressure [8, 9], and the Yb valence increased to be approximately 2.96 around 5 GPa with pressure. In $YbCu_{0.5}Ga_{1.5}$ and $YbCu_{1.5}Ga_{0.5}$ the Yb valence increased similarly from 2.4 and 2.84 at ambient pressure to approximately 2.9 around 10 GPa and 2.94 around 15 GPa, respectively. The results suggest that both $YbCu_{0.5}Ga_{1.5}$ and $YbCu_{1.5}Ga_{0.5}$ may be also in the Fermi liquid ground state at ambient pressure.

In Yb compounds, the Kondo temperature decreases

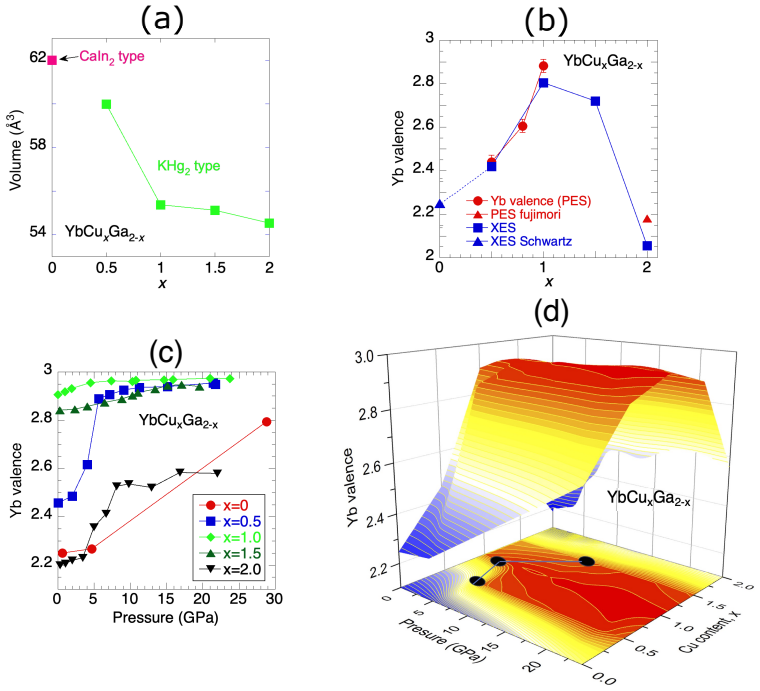

FIG. 6. (Color online) (a) Chemical composition, Cu content x dependence of the volume of $YbCu_xGa_{2-x}$. Here, we added the data of $YbGa_2$ although $YbGa_2$ have a different crystal structure of the $CaIn_2$ type. (b) Chemical composition dependence of the Yb valence obtained from the valence band spectra (closed circle) and the PFY-XAS spectra (closed square) as a function of x at ambient pressure except for the data at $x = 0$ (triangle) measured at 0.6 GPa [39]. The data at $x = 2.0$ (triangle and closed square) are taken from the Refs. [40, 53]. The errors of the data of XES (closed square) are within the size of the symbol. (c) Pressure dependence of the Yb valence in $YbCu_xGa_{2-x}$. (d) A summary of the chemical composition and pressure dependences of the Yb valence. In (d) closed circles at the bottom correspond to the points possibly being QCP.

with pressure and the Yb^{3+} state is favored. Some Yb compounds showed the pressure-induced change from the Fermi liquid ground state to the magnetic order state via QCP [18, 32, 57–59]. These systems show little change in the Yb valence at the pressures above QCP. QCP is defined to appear at low temperatures of nearly 0 K. The Yb valence normally decreases with decreasing temperature and thus, the valence fluctuation may be enhanced at low temperatures. However, a relative change in the Yb valence in the pressure dependence is considered to be similar to that at room temperature [58]. Therefore, YbCuGa may have QCP around $P_v = 2.5$ GPa. Present results also predict that the Yb compounds of $YbCu_{0.5}Ga_{1.5}$ and $YbCu_{1.5}Ga_{0.5}$ possibly have QCPs around $P_v = 5$ and $P_v = 10$ GPa, respectively. In $YbCu_{0.5}Ga_{1.5}$ temperature dependence of the electrical resistivity under pressure will show anomaly with the hysteresis and the divergent behavior of the A coefficient at P_v as observed in the Eu compounds [60, 61] if this system is in the Fermi liquid state at low temperatures. Such a study of the transport properties under pressure is expected.

$YbGa_2$ shows a large pressure-induced change in the Yb valence similar to the case of $YbCu_{0.5}Ga_{1.5}$ and therefore, we could expect a first-order valence transition also in $YbGa_2$ between 5 and 30 GPa. The first-order valence transition in $YbGa_2$ has not been confirmed yet due to too few data points in the measurements by Schwartz *et al.* [39].

In Fig. 6 (d) we show a summary of the chemical and pressure dependence of the Yb valence. At both the Cu content end sides of $x = 0$ and 2.0, the Yb valences are on the order of 2.2, divalent side at ambient pressure, while they are 2.8–2.9 around $x = 1.0$–1.5 around the region where the Cu and Ga contents are comparable. The result indicates that the unoccupied states above the Fermi level are little around $x = 1.0$–1.5 with small DOS hybridized weakly, while there are many unoccupied states at $x = 0$ and 2.0 with large DOS of Ga or Cu hybridized strongly [51]. In any case, pressure-induced the increase of the charge transfer from Yb to the unoccupied states of Ga or Cu, resulting in the increase of the Yb valence.

V. CONCLUSION

Pressure-induced changes in the electronic structure of $YbCu_xGa_{2-x}$ were studied by high-resolution XAS with a partial fluorescence mode at the Yb-L_3 absorption edge. In $YbCu_{0.5}Ga_{1.5}$ the first-order transition of the Yb valence was found around 5 GPa, where the Yb

valence increased largely from 2.6 to 2.9. The Yb valence of YbCuGa and $YbCu_{1.5}Ga_{01.5}$ successively increased up to 5 and 15 GPa, respectively, and it did not show a significant change above those pressures. In YbCuGa QCP around $P_v = 2.5$ GPa was suggested and the present results also predict a potential having QCPs of $P_v = 5$ GPa in $YbCu_{0.5}Ga_{1.5}$ and $P_v = 10$ GPa in $YbCu_{1.5}Ga_{01.5}$.

XRD study showed the structural phase transition in $YbCu_{0.5}Ga_{1.5}$ at the same pressure range of the valence transition, indicating the valence transition induced by the structural phase transition. We clarified the crystal structure of KHg_2-type at ambient pressure for $YbCu_{0.5}Ga_{1.5}$. The space group of $Pmmb$ with orthorhombic symmetry was suggested as a crystal structure at high pressures after the phase transition in $YbCu_{0.5}Ga_{1.5}$. $YbCu_{1.5}Ga_{0.5}$ and YbCuGa did not show the structural transition up to 15 GPa and 13 GPa, respectively.

The XAS spectra at the Cu-L absorption edge showed a shift of the edge energy to the lower incident energy with increasing x. At $x \leq 1$ the c–f hybridization occurred mainly between Yb and Ga, while the c–f hybridization between Yb and Cu may be enhanced at $x \geq 1.5$ due to both effects of the increase of the Cu DOS and decrease of the atomic distances between Yb and Cu. In $YbCu_xGa_{2-x}$ the main hybridization partner of Yb $4f$ electrons switched from Ga to Cu with increasing the Cu content around $x = 1$–1.5, where the c–f hybridization became minimum.

ACKNOWLEDGMENTS

The experiments were performed at Taiwan beamlines BL12XU and BL12B1 at SPring-8 under Proposals No. 2014B4257, No. 2015A4129, No. 2015A4258, No. 2015B4258, & No. 2015B4133 (corresponding proposals No. 2014-3-003 & No. 2015-2-033 of NSRRC) and also beamlines BL-7, BL-9 (Xe lamp), and BL-14 at HiSOR under Proposals No. 15-A-3, No. 16AG003, and No. 16AG004. We thank the N-BARD, Hiroshima University, for supplying the liquid helium. This work is supported by Grants in Aid for Scientific Research from the Japan Society for the Promotion of Science (Kiban C 15K05194, Kiban C 15K05190, & Houga 18K18743).

[1] J. M. Lawrence, P. S. Riseborough, and R. D. Parks, Valence fluctuation phenomena, Rep. Prog. Phys. **44**, 1 (1981).
[2] S. Doniach, The Kondo lattice and weak antiferromagnetism, Physca B & C **91**, 231 (1977).
[3] E. Bauer, Anomalous properties of Ce-Cu- and Yb-Cu-based compounds, Adv. Phys. **40**, 417 (1991).
[4] P. Coleman, C. Pépin, Qimiao Si, and R. Ramazashvili, How do Fermi liquids get heavy and die?, J. Phys.: Condens. Matter **13**, R273 (2001).
[5] H. v. Löhneysen, A. Rosch, M. Vojta, and P. Wölfle, Fermi-liquid instabilities at magnetic quantum phase transitions, Rev. Mod. Phys. **79**, 1015 (2007).
[6] P. Coleman, Heavy Fermions and the Kondo Lattice: A 21st Century Perspective, E. Pavarini, E. Koch, and P. Coleman eds. Many-body physics: From Kondo to Hubbard modeling and simulation Vol. **5** (Forschungszentrum Jülich, 2015, ISBN 978-3-95806-074-6).
[7] S. K. Malik, D. T. Adroja, B. D. Padalia, and R. Vijayaraghavan, Studies on the valence state of Yb in YbTGa (T = Cu, Pd and Pt) compounds through magnetic susceptibility measurements, Jpn. J. Appl. Phys. **26**, Suppl. 26-3 (1987).
[8] D. T. Adroja, S. K. Malik, B. D. Padalia, S. N. Bhatia, and R. Vijayaraghavan, Valence-fluctuation behavior of Yb ions in YbCuGa, Phys. Rev. B **42**, 2700 (1990).
[9] D. T. Adroja, B. D. Rainford, L. E. Miller, and S. K. Malik, Neutron scattering and transport studies of YbTGa compounds (T = Cu, Pd and Pt), Physica B **230-232**, 282 (1997).
[10] D. Rossi and R. Ferro, Ternary intermetallic RAgGa, RAuGa alloys (R = light rare earth and Yb), J. Alloys &d Compds. **317**, 521 (2001).
[11] U. Burkhardt, R Niewa, M. Schmidt, R. Gumeniuk, L. Vasylechko, and Y. Grin, Pressure dependence of Yb valence state of some ternary ytterbium - transition metal - gallides, HASYLAB Annual Report 2003.
[12] M. K. Reimann, H. Kohlmann, S. F. Matar, and R. Pöttgen, Ternary magnesium gallides–synthesis, crystal chemistry and properties of CaMgGa, SrMgGa, BaMgGa and YbMgGa, Z. Anorg. Allg. Chem. **649**, e202200361 (2022).
[13] U. Schwartz, M. Schmidt, R. Gumeniuk, W. Schnelle, M. Hanfland, K. Klementiev, and Yu. Grin, Chemical bonding and pressure-induced change of the electron configuration of ytterbium in β-$YbAgGa_2$, Z. Anorg. Allg. Chem. **630**, 122 (2004).
[14] R. Gumeniuk, E. Bischoff , U. Burkhardt, Yu. Prots, W. Schnelle, L. Vasylechko, M. Schmidt, Yu. Kuzma, and Yu. Grin, Order–disorder transition and valence state of ytterbiumin $YbAu_xGa_{2-x}$ ($0.26 < x < 1.31$), J. Solid State Chem. **182**, 3374 (2009).
[15] E. Bauer, Le Tuan, R. Hauser, E. Gratz, T. Holubar, G. Hilscher, H. Michor, W. Perthold, C. Godart, E. Alleno, and K. Hiebl, Evolution of a magnetic state in $YbCu_{5-x}Ga_x$, Phys. Rev. B **52**, 4327 (1995).
[16] U. Subbarao and S. C. Peter Crystal growth and properties of $YbCuGa_3$: First monoclinic system in the $RETX_3$ family, Cryst. Growth Des. **13**, 9653 (2013).
[17] Z. E. Brubaker, R. L. Stillwell, P. Chow, Y. Xiao, C. Kenney-Benson, R. Ferry, D. Popov, S. B. Donald, P. Söderlind, D. J. Campbell, J. Paglione, K. Huang, R. E. Baumbach, R. J. Zieve, and J. R. Jeffries, Pressure-dependent intermediate valence behavior in $YbNiGa_4$ and $YbNiIn_4$, Phys. Rev. B **98**, 214115 (2018).
[18] K. Matsubayashi, T. Hirayama, T. Yamashita, S. Ohara, N. Kawamura, M. Mizumaki, N. Ishimatsu, S. Watanabe, K. Kitagawa, and Y. Uwatoko, Pressure-induced valence

crossover and novel metamagnetic behavior near the antiferromagnetic quantum phase transition of $YbNi_3Ga_9$, Phys. Rev. Lett. **114**, 086401 (2015).
[19] K. Umeo, T. Otaki, Y. Arai, S. Ohara, and T. Takabatake, Pressure-induced quantum critical behavior and magnetic order in $YbNi_3Ga_9$ with a chiral crystal structure: ac calorimetric measurements up to 12 GPa, Phys. Rev. B **98**, 024420 (2018).
[20] H. Okamura, A. Takigawa, T. Yamasaki, E. D. Bauer, S. Ohara, Y. Ikemoto, and T. Moriwaki Contrasting pressure evolution of f-electron hybridized states in $CeRhIn_5$ and $YbNi_3Ga_9$: An optical conductivity study, Phys. Rev. B **100**, 105112 (2019).
[21] Y. Utsumi, D. Mondal, J. Fujii, I. Vobornik, S. Nakamura, D. Matković-Čalogović, and S. Ohara, Electronic structure of $Yb(Ni_{1-x}Co_x)_3Ga_9$ studied by angle-resolved photoelectron spectroscopy, J. Phys. Soc. Jpn. **89**, 044711 (2020).
[22] D. Mumbaraddi, V. Mishra, S. Lidin, and A. Mar, Minority report: Structure and bonding of $YbNi_3Ga_9$ and $YbCu_3Ga_8$ obtained in gallium flux, J. Solid State Chem. **311**, 123157 (2022).
[23] M. Schlüter and W. Jeitschko Ternary lanthanoid ruthenium gallides with a high gallium content: $Ln_2Ru_3Ga_{10}$ (Ln = Yb, Lu) with a new structure type and $LnRu_2Ga_8$ (Ln = La–Nd) with $CaCo_2Al_8$-type structure, Inorg. Chem. **40**, 6362 (2001).
[24] A. Rousuli, S. Nakamura, H. Sato, T. Ueda, Y. Matsumoto, S. Ohara, E. F. Schwier, T. Nagasaki, K. Mimura, H. Anzai, K. Ichiki, S. Ueda, K. Shimada, H. Namatame, and M. Taniguchi, Photoemission study of the electronic structure of the Kondo lattices $Yb_2Pt_6X_{15}$ (X = Al, Ga), Phys. Rev. B **96**, 045117 (2017).
[25] K. Hämäläinen, D. P. Siddons, J. B. Hastings, and L. E. Berman, Elimination of the inner-shell lifetime broadening in x-ray-absorption spectroscopy, Phys. Rev. Lett. **67**, 2850 (1991).
[26] K. Hämäläinen, C. C. Kao, J. B. Hasting, D. P. Siddons, L. E. Berman, V. Stojanoff, and S. P. Cramer, Spin-dependent x-ray absorption of MnO and MnF_2, Phys. Rev. B **46**,14274 (1992).
[27] J.-P. Rueff and A. Shukla, Inelastic x-ray scattering by electronic excitations under high pressure, Rev. Mod. Phys. **82**, 847 (2010).
[28] A. P. Hammersley, S. O. Svensson, M. Hanfland, A. N. Fitch, and D. Hausermann, Two-dimensional detector software: From real detector to idealised image or two-theta scan, High Press. Res. **14**, 235 (1996).
[29] Jana2006 program to analyze the crystal structures.
[30] V. Petricek, M. Dusek, and L. Palatinus, Crystallographic Computing System JANA2006: General features, Z. Kristallogr. **229**, 345 (2014).
[31] H. Yamaoka, Pressure dependence of the electronic structure of $4f$ and $3d$ electron systems studied by x-ray emission spectroscopy, High Press. Res. **36**, 262 (2016).
[32] H. Yamaoka, I. Jarrige, N. Tsujii, J.-F. Lin, N. Hiraoka, H. Ishii, and K.-D. Tsuei, Temperature and pressure-induced valence transitions in $YbNi_2Ge_2$ and $YbPd_2Si_2$, Phys. Rev. B **82**, 035111 (2010).
[33] H.-K. Mao and P. M. Bell, High-pressure physics: The 1-megabar mark on the ruby $R1$ static pressure scale, Science **191**, 851 (1976).
[34] K. Syassen, Ruby under Pressure, High Press. Res. **28**, 75 (2008).
[35] H. Yamaoka, Y. Zekko, I. Jarrige, J.-F. Lin, N. Hiraoka, H. Ishii, K.-D. Tsuei, and J. Mizuki, Ruby pressure scale in a low-temperature diamond anvil cell, J. Appl. Phys. **112**, 124503 (2012).
[36] M. Sawada, K. Yaji, M. Nagira, A. Kimura, H. Namatame, and M. Taniguchi, Design concept and performance of the soft x-ray beamline HiSOR-BL14, AIP Conf. Proc. **879**, 551 (2007).
[37] Peasons' Crystal Data Base; V. Y. Markiv, N. N. Belyavina, and T. I. Zhunkovskaya, The x-ray structure investigation of the Y-Cu-Ga system alloys and $RECu_2$-$REGa_2$ sections, Dopov. Akad. Nauk Ukr. RSR, Ser. A **2**, 80 (1982).
[38] Supplemental Material [url will be given by the editor side], which includes Refs. [39, 40, 48, 49, 51, 53, 62, 63]. We show (i) examples of the fit to the XRD pattern, results of structure refinements and final parameters used for the analyses, (ii) XAS spectra of $YbGa_2$ [39] and the estimated Yb valence, (iii) an explanation of the modified logistic curve, (iv) additional results of the resonant photoelectron spectroscopy for $YbCu_{0.5}Ga_{1.5}$, and (v) partial DOS of the band calculations.
[39] U. Schwarz, R. Giedigkeit, R. Niewa, M. Schmidt, W. Schnelle, R. Cardoso, M. Hanfland, Z. Hu, K. Klementiev, and Yu. Grin, Pressure-induced oxidation state change of ytterbium in $YbGa_2$, Z. Anorg. Allg. Chem. **627**, 2249 (2001).
[40] H. Yamaoka, A. Ohmura, N. Tsujii, H. Ishii, N. Hiraoka, H. Sato, and M. Sawada, Pressure-induced large valence transitions in Yb-Cu binary intermetallic systems, Phys. Rev. B **??**, ?? (2024).
[41] F. D. Murnaghan, The compressibility of media under extreme pressures, Proc. Natl. Acad. Sci. U.S.A. **30**, 244 (1944).
[42] Inorganic Crystal Structure Database (ICSD).
[43] H. Yamaoka, N. Tsujii, K. Yamamoto, A. M. Vlaicu, H. Oohashi, H. Yoshikawa, T. Tochio, Y. Ito, A. Chainani, and S. Shin, Systematic study of bulk sensitive spectroscopy in the valence transition of $YbInCu_4$-based compounds, Phys. Rev. B **78**, 045127 (2008).
[44] M. Finazzi, G. Ghiringhelli, O. Tjernberg, Ph. Ohresser, and N. B. Brookes, Radiationless Raman versus Auger behavior at the Cu L_3 resonance of CuO and Cu_2O, Phys. Rev. B **61**, 4629 (2000).
[45] H. Ebert, J. Stöhr, S. S. P. Parkin, M. Samant, and A. Nilsson, L-edge x-ray absorption in fcc and bcc Cu metal: Comparison of experimental and first-principles theoretical results, Phys. Rev. B **53**, 16067 (1996).
[46] P. Jiang, D. Prendergast, F. Borondics, S. Porsgaard, L. Giovanetti, E. Pach, J. Newberg, H. Bluhm, F. Besenbacher, and M. Salmeron, Experimental and theoretical investigation of the electronic structure of Cu_2O and CuO thin films on Cu(110) using x-ray photoelectron and absorption spectroscopy, J. Chem. Phys. **138**, 024704 (2013).
[47] Y. Utsumi, H. Sato, H. Kurihara, H. Maso, K. Hiraoka, K. Kojima, K. Tobimatsu, T. Ohkochi, S. Fujimori, Y. Takeda, Y. Saitoh, K. Mimura, S. Ueda, Y. Yamashita, H. Yoshikawa, K. Kobayashi, T. Oguchi, K. Shimada, H. Namatame, and M. Taniguchi, Conduction-band electronic states of $YbInCu_4$ studied by photoemission and soft x-ray absorption spectroscopies, Phys. Rev. B **85**, 114143 (2011).
[48] H. Yamaoka, P. Thunström, N. Tsujii, I. Jarrige, K. Shi-

mada, M. Arita, H. Iwasawa, H. Hayashi, J. Jiang, H. Namatame, M. Taniguchi, N. Hiraoka, H. Ishii, K.-D. Tsuei, M. Giovannini, and E. Bauer, Electronic structure and the valence state of Yb_2Pd_2Sn and $YbPd_2Sn$ studied by photoelectron and resonant x-ray emission spectroscopies, Phys. Rev. B **86** 085137 (2012).

[49] H. Yamaoka, P. Thunström, N. Tsujii, K. Katoh, Y. Yamamoto, E. F. Schwier, K. Shimada, H. Iwasawa, M. Arita, I. Jarrige, N. Hiraoka, H. Ishii, K.-D. Tsuei, and J. Mizuki, Electronic structure of ferromagnetic heavy fermion, YbPdSi, YbPdGe, and YbPtGe studied by photoelectron spectroscopy, x-ray emission spectroscopy, and DFT + DMFT calculations, J. Phys.: Condens. Matter **29**, 475502 (2017).

[50] J. J. Yeh and I. Lindau, Atomic subshell photoionization cross sections and asymmetry parameters: $1 \leq Z \leq 103$, At. Data Nucl. Data Tables **32**, 1 (1985).

[51] I. Jarrige, H. Yamaoka, J.-P. Rueff, J.-F. Lin, M. Taguchi, N. Hiraoka, H. Ishii, K.-D. Tsuei, K. Imura, T. Matsumura, A. Ochiai, H. S. Suzuki, and A. Kotani, Unified understanding of the valence transition in the rare-earth monochalcogenides under pressure, Phys. Rev. B **87**, 115107 (2013).

[52] E. R. Ylvisaker, J. Kuneš, A. K. McMahan, and W. E. Pickett, Charge fluctuations and the valence transition in Yb under pressure, Phys. Rev. Lett. **102**, 246401 (2009).

[53] A. Fujimori, T. Shomizu, and H. Yasuoka, Photoemission study of valence fluctuation in $YbCu_2$, Phys. Rev. B **35**, 8945 (1987).

[54] L. Moreschini, C. Dallera, J. J. Joyce, J. L. Sarrao, E. D. Bauer, V. Fritsch, S. Bobev, E. Carpene, S. Huotari, G. Vankó, G. Monaco, P. Lacovig, G. Panaccione, A. Fondacaro, G. Paolicelli, P. Torelli, and M. Grioni, Comparison of bulk-sensitive spectroscopic probes of Yb valence in Kondo systems, Phys. Rev. B **75**, 035113 (2007).

[55] H. Yamaoka, A. Ohmura, Y. Furue, N. Tsujii, H. Ishii, and N. Hiraoka, Direct observation of pressure-induced Yb valence transition in $YbInCu_4$, J. Phys. Soc. Jpn. **90**, 124801 (2021).

[56] B. Tegomo Chiogo, N. P. Martin, L. V. B. Diop, B. Malaman, D. Malterre, F. Baudelet, L. Nataf, and T. Mazet, Temperature and pressure dependence of the Yb valence state in $YbMn_{\sim 0.17}Si_{\sim 1.89}$, J. Appl. Phys. **132**, 205902 (2022).

[57] H. Yamaoka, N. Tsujii, Y. Utsumi, H. Sato, I. Jarrige, Y. Yamamoto, J.-F. Lin, N. Hiraoka, H. Ishii, K.-D. Tsuei, and J. Mizuki, Valence transitions in the heavy-fermion compound YbCuAl as a function of temperature and pressure, Phys. Rev. B **87**, 205120 (2013).

[58] H. Sato, H. Yamaoka, Y. Utsumi, H. Nagata, M. A. Avila, R. A.. Ribeiro, K. Umeo, T. Takabatake, Y. Zekko, J. Mizuki, J.-F. Lin, N. Hiraoka, H. Ishii, K.-D. Tsuei, H. Namatame, and M. Taniguchi, Pressure-induced valence change of $YbNiGe_3$ investigated by resonant x-ray emission spectroscopy at the Yb L_3 edge, Phys. Rev. B **89**, 045112 (2014).

[59] W. B. Jiang, L. Yang, C. Y. Guo, Z. Hu, J. M. Lee, M. Smidman, Y. F. Wang, T. Shang, Z. W. Cheng, F. Gao, H Ishii, K. D. Tsuei, Y. F. Liao, X. Lu, L. H. Tjeng, J. M. Chen, and H. Q. Yuan, Crossover from a heavy fermion to intermediate valence state in noncentrosymmetric $Yb_2Ni_{12}(P, As)_7$, Sci. Rep. **5**, 17608 (2015).

[60] F. Honda, K. Okauchi, A. Nakamura, D. Aoki, H. Akamine, Y. Ashitomi, M. Hedo, T. Nakama, and Y. Ōnuki, Pressure evolution of characteristic electronic states in $EuRh_2Si_2$ and $EuNi_2Ge_2$, J. Phys. Conf. Ser. **807**, 022004 (2017).

[61] Y. Ashitomi, M. Kakihana, F. Honda, A. Nakamura, D. Aoki, Y Uwatoko, M. Nakashima, Y. Amako, T. Takeuchi, T. Kida, T. Tahara, M. Hagiwara, Y. Haga, M. Hedo, T. Nakama, and Y. Ōnuki, Magnetic properties and effect of pressure on the electronic state of $EuCo_2Ge_2$, Physica B **536**, 192 (2018).

[62] Wien2k: An APW + lo program for calculating the properties of solids.

[63] P. Blaha, K. Schwarz, F. Tran, R. Laskowski, G. K. H. Madsen, and L. D. Marks, WIEN2k: An APW + lo program for calculating the properties of solids, J. Chem. Phys. **152**, 074101 (2020).